Industrial Chemistry
& Materials

PAPER

View Article Online
View Journal

Cite this: DOI: 10.1039/d6im00020g

MOF-based homogeneous ion exchange membranes for high-efficiency magnesium–lithium separation

Tong Mu,†[ab] Geting Xu,†[ab] Zhihang Xia,[ab] Hao Qian,[ab] Yangbo Qiu,[c] Wanji Zhou,[d] Jiahao Yu,[ab] Yunfang Gao, *[ae] Junbin Liao*[ab] and Jiangnan Shen *[ab]

Received 15th January 2026,
Accepted 8th April 2026

DOI: 10.1039/d6im00020g

rsc.li/icm

The rapidly increasing demand for lithium resources has driven significant advances in membrane-based separation technologies for extracting lithium from salt lake brines. However, conventional polymer membranes often suffer from key challenges of permeability and perm-selectivity. Herein, we have constructed a functional sieving layer for monovalent-ion-selective membranes through interfacial polymerization by incorporating UiO-66-NH_2 with poly(diallyldimethylammonium chloride) (PDADMAc) polyelectrolyte, which has been successfully applied in electrodialysis processes for efficient Li^+/Mg^{2+} separation. The fabricated membranes have facilitated Li^+ transport while blocking Mg^{2+} effectively, owing to the synergistic effect between stable electrostatic repulsion and sufficient functional transport channels. Experimental results have shown that the membranes have exhibited extremely high permeation fluxes of monovalent ions (Li^+/Na^+): the permeation flux of Li^+ reaches 1.59×10^{-8} mol cm^{-2} s^{-1}, the permeation flux of Na^+ reaches 1.48×10^{-8} mol cm^{-2} s^{-1}, whereas the corresponding Mg^{2+} flux is only 0.40×10^{-8} mol cm^{-2} s^{-1}. These results correspond to high separation selectivities of $P_{Na^+/Mg^{2+}} = 26.2$ and $P_{Li^+/Mg^{2+}} = 32.2$, which markedly outperform commercial membranes and those reported in published studies. It also provides a novel electrodialysis strategy for Li^+/Mg^{2+} separation by leveraging MOF-based membranes, offering valuable insights for the efficient recovery of monovalent ion resources.

Keywords: Electrodialysis-based monovalent/multivalent ion sieving; Metal-organic framework; Interfacial polymerization; High Li^+ permeation flux; High perm-selectivity.

1 Introduction

Given its low density and high chemical potential, lithium is crucial for high-energy-density batteries and energy storage systems, demonstrating significant application potential.[1–5] Lithium and its compounds are widely utilized across industries such as the information industry, energy industry, and transportation industry, serving as an indispensable component in production and daily life.[6,7] Consequently, the extraction from salt lake brines, which hold 59–61.8% of the global proven-lithium resources (approximately 14 million tons),[8–10] has become a major focus for securing these essential materials. However, selective lithium extraction from salt lakes is challenging due to the complex brine composition (*e.g.*, Li^+, Na^+, K^+, Ca^{2+}, Mg^{2+}) and the extremely high Mg^{2+}/Li^+ ratio.[11] The highly similar chemical properties of magnesium ions to lithium ions (Li^+)[12–14] represent a critical issue that needs to be addressed in the selective extraction of lithium. Existing methods such as precipitation[15–17] and solvent extraction[18,19] face limitations such as high energy consumption, stringent environmental requirements, and severe pollution, which shows the critical need for advanced separation technologies, such as membrane-based processes. Therefore, developing novel and more efficient approaches for lithium extraction from salt lakes is imperative.

As an emerging membrane separation technology, electrodialysis (ED) relies on the directional migration of ions under an applied electric field, which results in its relatively low energy consumption as a “phase-invariant process”.[20,21] For monovalent/multivalent separation, the key component

---

[a] College of Chemical Engineering, Zhejiang University of Technology, Hangzhou 310014, China. E-mail: Gaoyf@zjut.edu.cn, Liaojb@zjut.edu.cn, Shenjn@zjut.edu.cn
[b] State Key Laboratory of Advanced Separation Membrane Materials, National Key Laboratory of Green Chemical Synthesis and Transformation Technology, Zhejiang University of Technology, Hangzhou 310014, China
[c] Department of Civil Engineering, The University of Hong Kong, Pokfulam, Hong Kong, SAR 999077, PR China
[d] Salt Lake Chemical Engineering Research Complex, School of Chemical Engineering, Qinghai University, Xining 810016, Qinghai, China
[e] Key Research and Development Program of Zhejiang Province, Zhejiang University of Technology, Hangzhou 310014, China

† Co-first authors.

in ED is the monovalent-selective separation ion exchange membranes. Typically, the research on monovalent-selective separation membranes has focused on the construction of positively charged layers on the surface of the membrane, the incorporation of special materials, *etc.* Functional materials with tailored nanostructures (such as crown ethers,[22–24] metal–organic frameworks (MOFs),[23–25] and covalent organic frameworks (COFs)) are introduced. Wang *et al.* fabricated crown ether-functionalized polymer membranes by incorporating 12-crown-4 rings into cellulose triacetate polymer networks, achieving an ultra-high Li^+/Mg^{2+} separation factor of ~872 and a Li^+ flux of 22.6 μmol m^{-2} s^{-1}, demonstrating exceptional Li^+/Mg^{2+} separation performance.[22] Additionally, Hu *et al.* proposed a novel coordination-driven *in situ* self-assembly strategy to fabricate ZIF-8 nanocrystal hybrid thin-film nanocomposite (TFN) membranes with remarkable desalination performance. The significantly reduced surface roughness and enhanced surface hydrophilicity endowed the TFN-ZIF-8 membranes with excellent antifouling properties.[24] A series of studies have confirmed the great potential of functional materials in the field of magnesium–lithium separation.

Among these, MOFs, which are two- or three-dimensional porous networks constructed from metal nodes and organic linkers, have been proven to possess great potential for ion sieving.[26] A synergistic strategy involves incorporating MOFs with organic polymers, which not only can significantly enhance membrane stability and mechanical properties but also endow advanced functions.[26] In this context, the UiO-66 family of metal–organic frameworks has been reported to be applied in ion-exchange membranes, exhibiting excellent monovalent ion sieving performance.[27–29] Additionally, their appeal is further heightened by the tunability of organic linkers, allowing for the deliberate introduction of functional groups and charges,[30] which presents a substantial opportunity for designing next-generation ion-sieving membranes. Current research on UiO-66 metal–organic frameworks (MOFs) remains largely confined to polymer blending and simple interfacial polymerization. The blending approach, however, often causes pore blockage by the polymer matrix, impairing the functionality of the MOFs. Conversely, simple interfacial polymerization struggles to yield stable and uniform MOF layers due to challenges such as particle agglomeration, crystalline defects, and the lack of functional groups for effective anchoring. Moreover, structural imperfections in the UiO-66 layer itself frequently hinder the efficient capture of target ions. To overcome these limitations, we have developed a novel interfacial polymerization composite membrane featuring an intermediate adhesion layer and a main functional layer composed of a polyelectrolyte/MOF complex. This innovative architecture concurrently resolves the issues of poor functional layer adhesion, inaccessible MOF pores, and insufficient charge repulsion.

In this study, we prepared innovative monovalent-selective cation exchange membranes with a stable positively charged surface layer using sulfonated polyethersulfone (SPES) as the base membrane. By utilizing pre-synthesized UiO-66-NH_2 MOF materials and poly(diallyldimethylammonium chloride) (PDADMAc) polyelectrolyte materials containing abundant stable positively charged groups,[30] with PEI as the interlayer, the as-prepared membranes have features of a relatively uniform positively charged surface layer, along with low electrical resistance and a relatively stable overall structure. During the ED process, the membrane exhibits excellent monovalent sieving performance ($P_{Na^+/Mg^{2+}}$ = 26.2 and $P_{Li^+/Mg^{2+}}$ = 32.2) and high ion permeability ($J_{Li^+} = 1.59 \times 10^{-8}$ mol cm^{-2} s^{-1}, $J_{Na^+} = 1.48 \times 10^{-8}$ mol cm^{-2} s^{-1}), confirming that the strategy shows strong electrostatic repulsion towards multivalent ions and selective permeability to monovalent ions (Table 1).

2 Results and discussion

2.1 Membrane surface morphology

To analyze the morphological changes on the membrane surface, scanning electron microscopy (SEM) and atomic force microscopy (AFM) were employed for membrane characterization (Fig. 1 and S1). SPES-1 exhibited a disordered arrangement of small pores, similar to conventional SPES membranes.[31] In contrast to the SPES-1 substrate membrane (a), after the formation of the PEI interlayer (b), obvious wrinkled polyelectrolyte layers were observed on the membrane surface. Furthermore, after modification with the U/P layer, the membrane surface initially presented a spherical agglomerated structure, which corresponds to the morphological characteristics of UIO-66-NH_2,[32] thus verifying the successful introduction of functional MOFs onto the PEI functional interlayer. The block-like structures observed on the membrane surface are attributed to the increased reaction time, which leads to variations in the thickness and morphology of the functional

Table 1 Physico-chemical properties of the prepared membranes

CEM	Surface area resistance (Ω)	SR (%)	Water uptake (%)	IEC
SPES	2.2 ± 0.1	2.3 ± 0.3	21.9 ± 0.9	3.51 ± 0.5
SPES/PEI	3.4 ± 0.2	5.2 ± 0.5	23.9 ± 1.0	3.42 ± 0.4
SPES/PEI/U/P-5	4.7 ± 0.5	12.9 ± 0.8	22.5 ± 1.0	3.47 ± 0.3
SPES/PEI/U/P-15	5.5 ± 0.5	13.6 ± 0.6	30.8 ± 1.0	3.43 ± 0.5
SPES/PEI/U/P-30	6.1 ± 0.4	15.5 ± 0.7	34.4 ± 0.9	3.47 ± 0.4

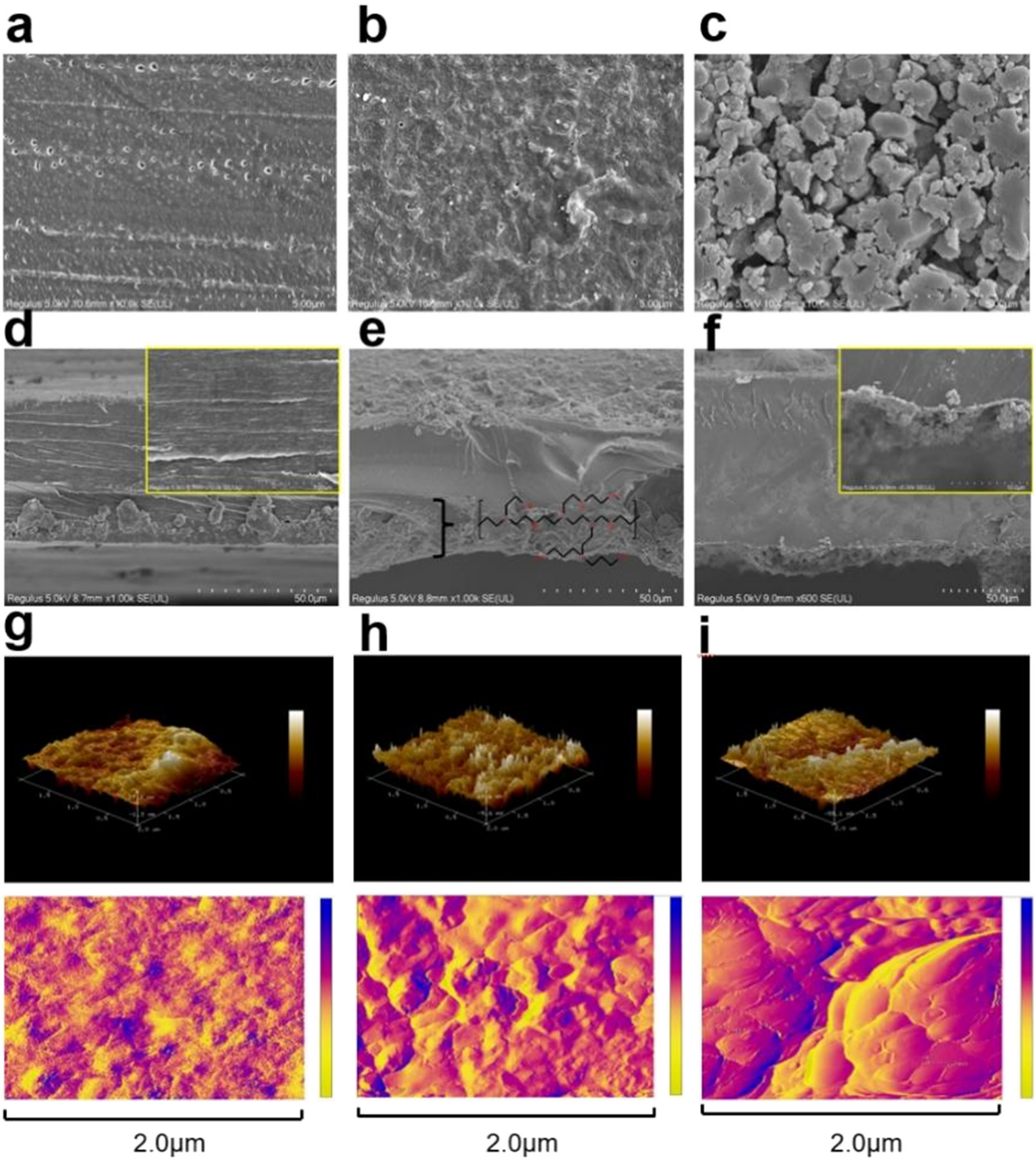

Fig. 1 SEM images of membranes (a) SPES-1, (b) SPES/PEI-2, and (c) SPES/PEI/U/P-*n*; surface SEM images of (d) SPES-1, (e) SPES/PEI-2, and (f) SPES/PEI/U/P-*n* cross-section (the content within the box represents a cross-sectional view of the membrane at a finer scale); and AFM images of membranes (g) SPES-1, (h) SPES/PEI-2, and (i) SPES/PEI/U/P-*n* (the colored areas represent the planar structure of the membrane material, while the remainder depicts its three-dimensional configuration).

layer (due to enhanced attachment of MOF/PDDA), and the variation in the thickness of the functional layer corresponds to the introduction of more quaternary ammonium groups and a greater number of MOF pore structures, which enhance Li^+ permeation while reducing Mg^{2+} permeation through electrostatic repulsion and the construction of ionic channels,[28] respectively, corresponding to higher Li^+ perm-selectivity and greater flux (Table 2).

Table 2 Perm-selectivity and ion flux of different membranes

Current density (mA cm^{-2})	Name	$J(Li^+)$ (mol cm^{-2} s^{-1})	$J(Mg^{2+})$ (mol cm^{-2} s^{-1})	Perm-selectivity
2.5	SPES-1	$1.06 \pm 0.04 \times 10^{-8}$	$0.63 \pm 0.05 \times 10^{-8}$	1.8 ± 0.2
	SPES/PEI-2	$1.10 \pm 0.05 \times 10^{-8}$	$0.45 \pm 0.04 \times 10^{-8}$	5.2 ± 0.3
	SPES/PEI/U/P-5	$1.31 \pm 0.04 \times 10^{-8}$	$0.61 \pm 0.04 \times 10^{-8}$	6.6 ± 0.4
	SPES/PEI/U/P-15	$1.51 \pm 0.03 \times 10^{-8}$	$0.57 \pm 0.04 \times 10^{-8}$	23.3 ± 0.7
	SPES/PEI/U/P-30	$1.59 \pm 0.04 \times 10^{-8}$	$0.41 \pm 0.03 \times 10^{-8}$	32.2 ± 1.4
5	SPES/PEI/U/P-30	$1.63 \pm 0.04 \times 10^{-8}$	$1.47 \pm 0.03 \times 10^{-8}$	13.9 ± 0.5

The surface roughness phase diagram demonstrates a consistent trend. The initially prepared SPES-1 substrate membrane exhibits a smooth surface, whereas the introduction of PEI and MOF/PDDA leads to significant changes in roughness, presenting a sharper and more pronounced topography. These observations correspond to a thicker functional surface layer of the membrane material (for specific SEM and AFM images of the different membranes, please refer to the SI).

2.2 Physicochemical properties

After undergoing tests for ion exchange capacity (IEC), resistance (R), water uptake (WU), and swelling ratio (SR) (the testing procedures are detailed in the SI), the results are presented in Fig. 2. The evaluated ion exchange capacity (IEC), a key determinant of a membrane's intrinsic ion exchange capability, was measured for the series of membranes. All the samples exhibited exceptionally high IEC values of approximately 3.5 mmol g^{-1}. This high IEC directly contributed to the superior ion flux observed in subsequent tests, which, in turn, is a critical factor influencing the membranes' perm-selectivity. In addition, the perm-selectivity of membranes is also influenced by the hydrophilic–hydrophobic properties of the membrane surface. Traditionally, the more hydrophobic the membranes, the stronger their repulsive effect on ions (in this study, this category of ions is defined as Mg^{2+}); however, a more hydrophilic membrane can also promote the transport of monovalent ions to a certain extent. Compared to Mg^{2+}, Li^+ requires the removal of fewer hydration shells for transmembrane transport and must overcome a lower dehydration energy barrier. Therefore, membranes with enhanced hydrophilicity can, to some extent, increase the

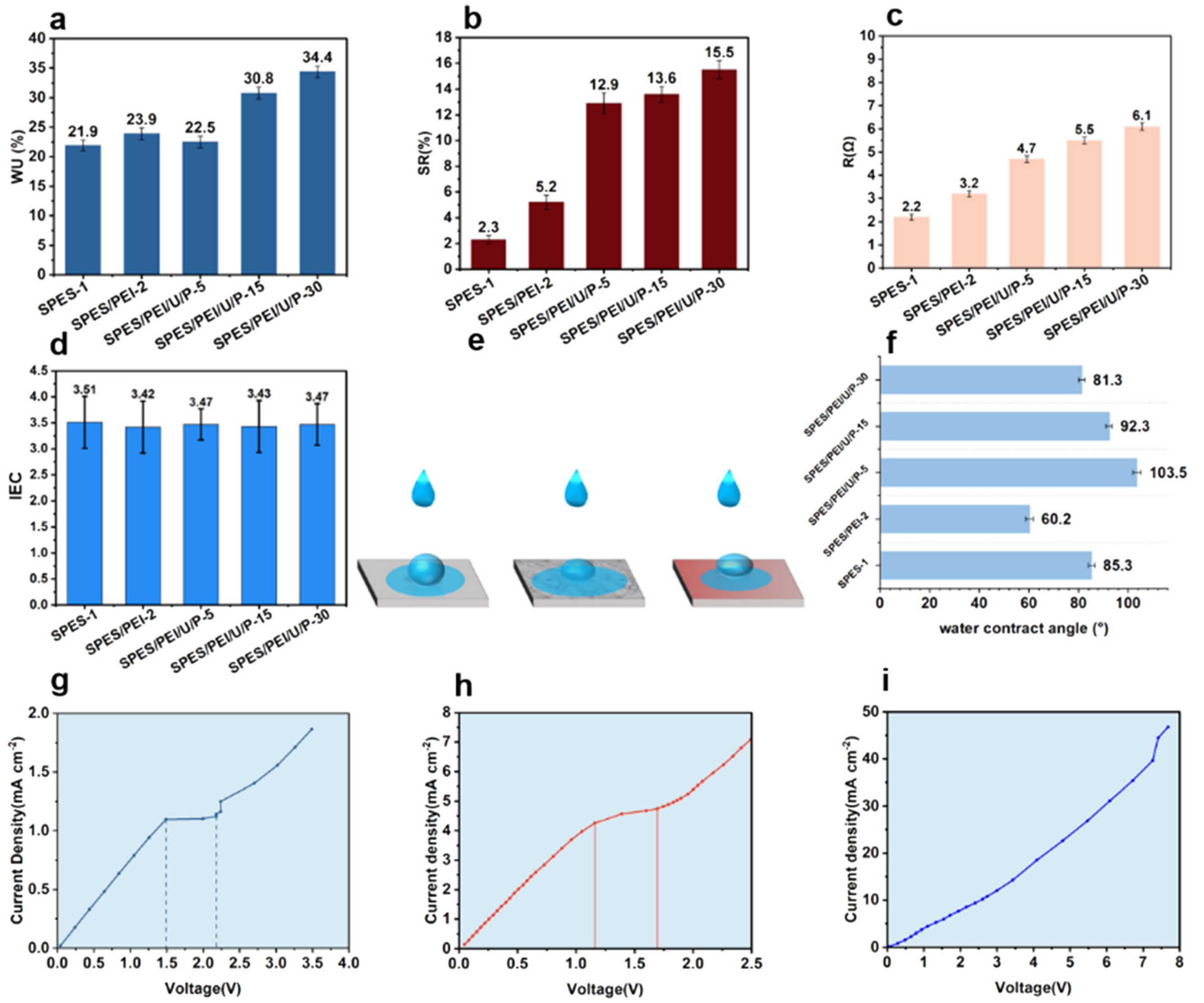

Fig. 2 (a) Resistance, (b) WU, (c) SR, (d) IEC, (e) water contact process and (f) water contract angle; (g) *U–I* curve of FUJI CEM; (h) *U–I* curve of SPES-1; (i) *U–I* curve of SPES/PEI/U/P-30.

migration rate of Li^+ during the transport process. The hydrophilicity (water uptake, WU) and swelling ratio (SR) of different membranes were measured. It was found that the initial SPES membrane exhibited a relatively high WU (21.9%) and a low SR (2.3%). WU is attributed to the inherent property of sulfonate groups, which generally possess strong hydrophilicity.[40,41] The low SR provides a basis for the structural and performance stability of the substrate membrane in interfacial polymerization. After modification with the PEI interlayer, the hydrophilicity of the membrane underwent significant changes, specifically, the WU increased from 21.9% to 23.0% and the SR rose to 5.2%. This change is attributed to the large number of amino groups in the PEI, which also have a certain degree of hydrophilicity.[42] Following the polymerization of the U/P layer, both WU and SR increased to varying degrees. This can be ascribed to the abundant quaternary ammonium groups in the polyelectrolyte material; as strongly hydrophilic groups, quaternary ammonium groups exhibit much stronger hydrophilicity than primary and secondary amines.[43] Moreover, as the reaction time increased, both WU and SR further increased. This variation is consistent with the change in the thickness of the layer observed by SEM, reflecting that the thickness of the U/P layer increased significantly with prolonged reaction time, which provides stronger electrostatic repulsion for the membrane in subsequent selectivity tests. In addition, the change in resistance follows the same trend. The low resistance of the substrate membrane (2.2 Ω cm^2) and the increase in resistance with the introduction of the functional layer also indicate the change in the thickness of the functional layer. Notably, the membrane obtained with the longest reaction time exhibited a resistance of only 6.1 Ω cm^2, which guarantees faster transport and higher flux of monovalent ions.

For the water contact angle measurement, the water contact angle was adopted as a direct characterization to evaluate the hydrophilic–hydrophobic properties of the membrane surface. It can be observed that the variation trend of the water contact angle is consistent with that of hydrophilicity. SPES/PEI-2 exhibits the smallest water contact angle (60.2°), corresponding to the highest hydrophilicity of this membrane. After the synthesis of the U/P layer, the water contact angle first increases to a certain extent and then gradually decreases, which is consistent with the trend of hydrophilicity first decreasing and then increasing. This confirms that the membrane becomes more hydrophilic as the reaction time increases, which is also attributed to the increased modification amount of quaternary ammonium groups, driving the membrane surface toward a more hydrophilic direction. Furthermore, regarding the introduction of the U/P layer, when the reaction time is short (*i.e.*, for the SPES/PEI/U/P-5 membrane), the hydrophilicity decreases to a certain extent, which is accompanied by an increase in the water contact angle. However, when considering the influence of hydrophobicity on ion selectivity tests, the ion selectivity shows that increased hydrophilicity leads to a higher Li^+ flux and a stronger rejection of Mg^{2+}, which corresponds to an overall improvement in selectivity.

In addition, to evaluate the mass transfer capacity, operating limits, and safety performance of the membrane, a limiting current density test of the ion exchange membrane was conducted. Generally, the voltage–current (U–I) curve exhibits three characteristic regions, namely one ohmic region and two non-ohmic regions. In the ohmic region, the current density increases rapidly with the rise in voltage, whereas in the non-ohmic regions, the current density eventually levels off due to the stabilization of the electrolyte concentration gradient. During the tests performed in this study, the commercial membrane and the SPES-1 membrane showed obvious inflection points, indicating that their limiting current densities have clear values. However, the U–I curve of SPES/PEI/U/P-30 differs from that of the commercial membrane, showing a distinct linear variation. This proves that the membrane can operate stably under relatively high current densities. The MOF pores on the membrane surface reduce the concentration polarization during the mass transfer process. Meanwhile, due to its lower resistance and higher ion flux, the membrane is suitable for various working conditions under relatively high current densities.

2.3 Chemical characterization of functional membranes and MOFs

For the characterization of the chemical composition of the membrane and the functional layer, FT-IR spectroscopy was used to determine the chemical bond, and the results are shown in Fig. 3. For SPES/PEI/U/P-*n*, the peak appearance at 3413.38 cm^{-1} corresponds to the polarized absorption peak of secondary amine.[38] The shift of the peak position wavelength corresponds to the appearance of the amide structure. This also demonstrates that TMC forms a stable amide bond structure with hydrogen on the PEI amino group and hydrogen on UIO-66-NH_2, which indicates that the interfacial polymerization process will stabilize the existence of PEI and the functional layer on the membrane surface. In addition, in order to examine the combination of the carboxyl terminal of the MOF structure and free hydrogen ions on the PDADMAc methyl group, the peak of the carboxylic acid dimer often appears at 3200–2500 cm^{-1} because carboxylic acid easily forms a dimer through hydrogen bonding. Therefore, the existence of peaks at 2957.71 cm^{-1} and 2924.53 cm^{-1} in the spectrum of SPES/PEI/U/P/-*n* can judge the structure of the dimer formed by SPES/PEI/U/P/-*n* and polyelectrolyte. The peak shape of the formed carboxylic acid dimer structure often shows two peaks with close positions, so it can be preliminarily demonstrated that the binding mode of UIO-66-NH_2 and PDADMAc is a hydrogen bond. In the XPS analysis diagram of SPES-1, the peak on the left corresponds to the polarized absorption peak of the S═O bond (sulfonic acid often shows a broad peak or two peaks at 531–533 eV), which proves the

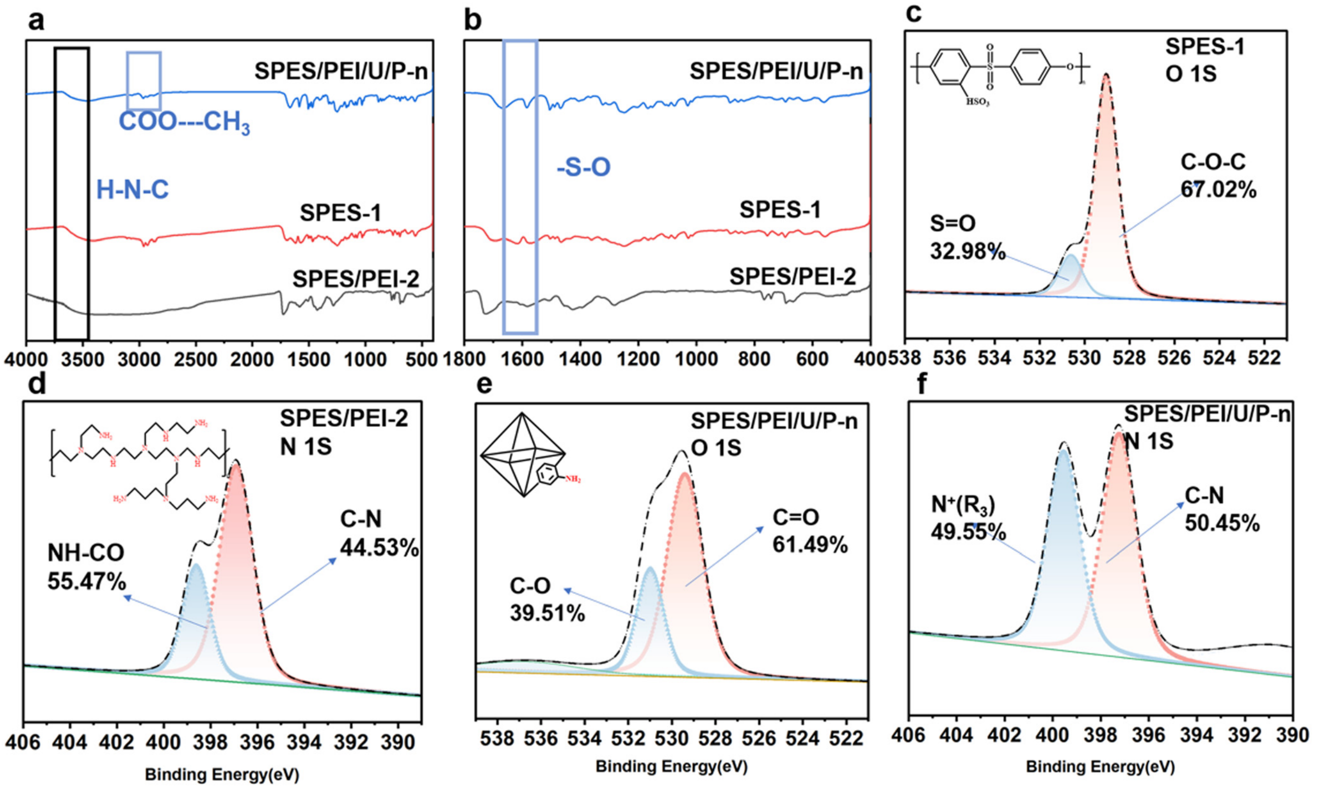

Fig. 3 Infrared spectra and XPS spectra. (a) FT-IR in the range of 400–4000 cm^{-1} and (b) in the range of 400–1800 cm^{-1}; (c) O 1s spectrum of SEPS; (d) N 1s spectrum of SPES/PEI-2; (e) O 1s spectrum of SPES/PEI/U/P-*n*; (f) N 1s spectrum of SPES/PEI/U/P-*n*.

success of sulfonation contained in the SPES polymer. Meanwhile, the ether bond peak on the right proves the stability of the polymer main chain structure after sulfonation. For SPES/PEI-2, the spectra of N 1s show that the peak with a larger area on the right side corresponds to the C–N bond in the PEI backbone structure, which proves the stable existence of the PEI polymer material. In particular, the polarized absorption peak of the amide bond appears at the same time on the left side. The existence of this peak successfully proves the successful combination of PEI and TMC, and its stable existence on the membrane surface. In the O 1s spectrum of SPES/PEI/U/P-*n*, the peak at about 528 eV on the right side corresponds to the ether bond of the SPES polymer backbone, while the peak at about 531 eV on the left side should correspond to the polarized absorption peak of C═O on the carboxyl group.[39] It is worth noting that the peak displayed at the position of higher binding energy should be the peak displayed by the hydrogen bond structure formed by the hydroxyl group and free hydrogen ion at the end of the polyelectrolyte backbone. Because of the existence of the hydrogen bond, this type of peak will show a large shift on the spectrum. At the same time, its peak area is small, which also shows that the content of functional layer structure is reasonable to some extent. On the N 1s spectrum of SPES/PEI/U/P-*n*, the obvious absorption peak corresponding to the quaternary amine group on the left should correspond to the existence of the PDADMAc polyelectrolyte material, and another peak with a larger area at the lower binding energy position corresponds to the incomplete reaction of amino groups on the MOF structure and PEI structure. In particular, the peak with lower binding energy on the right may correspond to the amide bond formed by the reaction of amino groups on the MOF with acyl chloride. The appearance of this peak also proves the successful synthesis of the U/P functional layer and the successful combination with the membrane.

For the characterization of UiO-66-NH_2, the XRD pattern exhibits strong and sharp diffraction peaks with no significant peak shifting, confirming its highly crystalline structure and intact crystal form (see SI for details). The BET analysis results demonstrate that the as-synthesized UiO-66-NH_2 MOFs possess an inherent pore size of 0.8 ± 0.1 nm, which aligns well with the intrinsic hydrated diameters of Li^+ and Mg^{2+} (approximately 0.764 nm and 0.825 nm, respectively) in the magnesium–lithium separation process. This congruence provides feasible pore channel support for the separation of magnesium and lithium ions (Fig. 4).

2.4 High cation permselective separation performance

The selectivity results obtained from the electrodialysis tests are presented below. Compared with SPES-1, SPES/PEI-2 contains an abundance of positively charged groups, which are responsible for its ion selectivity. Specifically, it shows a

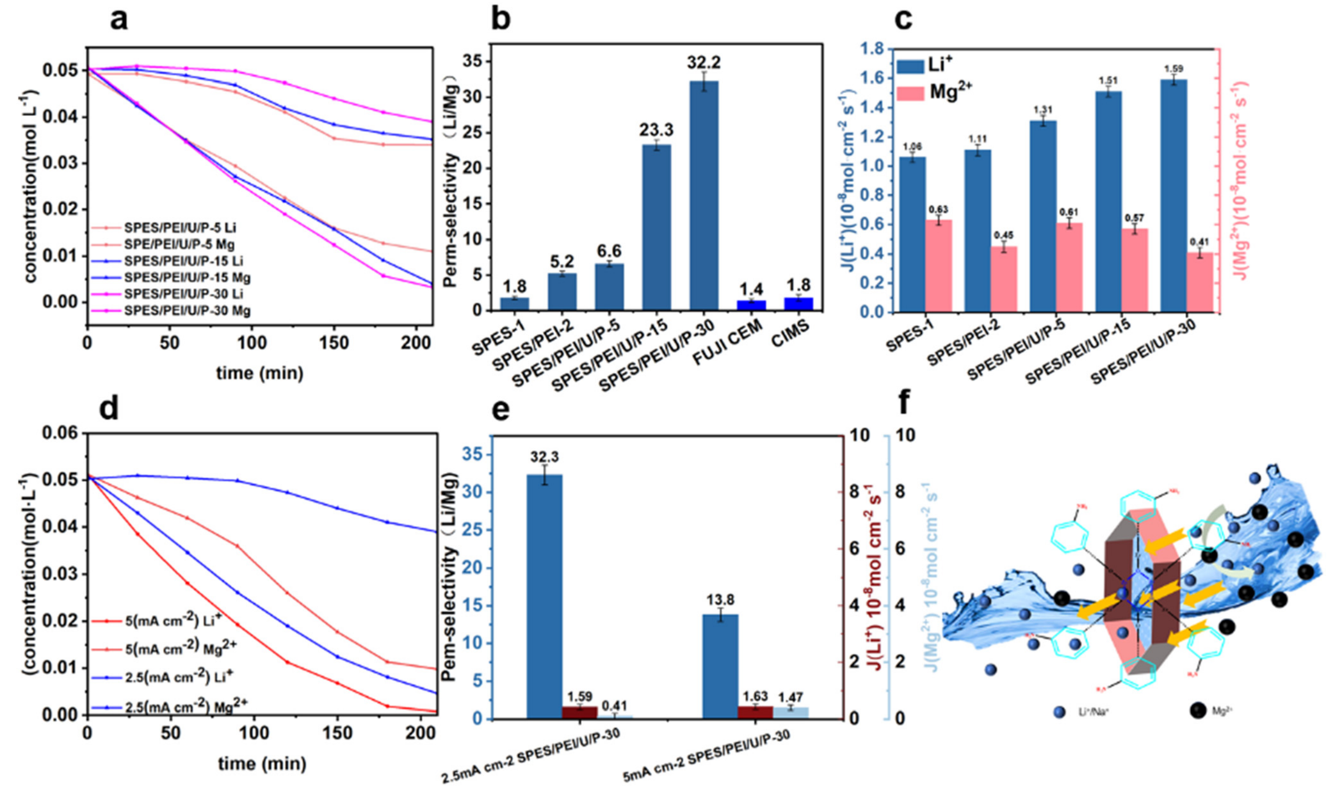

Fig. 4 (a) Concentration evolution of Li^+ and Mg^{2+} ion in DC of EDs fabricated with SPES/PEI/U/P-*n* in different reaction times; (b) Mg^{2+}/Li^+ perm-selectivity of different membranes; (c) ion flux of Mg^{2+} and Li^+ in ED; (d) concentration evolution of Li^+ and Mg^{2+} ion in DC of Eds of SPES/PEI/U/P-30 under different current densities; (e) Li^+/Mg^{2+} perm-selectivity and ion flux under different current densities; (f) schematic diagram of ion transport through MOFs.

significant improvement in perm-selectivity (1.8–5.2) and a notable decrease in Mg^{2+} ion flux (0.63×10^{-8}–0.44×10^{-8} mol cm^{-2} s^{-1}). This indicates the successful introduction of PEI, which not only acts as a supporting layer for the U/P layer but also exerts a certain electrostatic repulsion effect. For SPES/PEI/U/P-*n*, compared with SEPS/PEI-2, their perm-selectivity and ion flux also exhibit significant changes. Specifically, the perm-selectivity increases from 5.18 to a maximum of 32.2, while the Li^+ flux rises from 1.09×10^{-8} mol cm^{-2} s^{-1} to 1.59×10^{-8} mol cm^{-2} s^{-1}. Correspondingly, the Mg^{2+} flux decreases from 0.44×10^{-8} mol cm^{-2} s^{-1} to a minimum of 0.40×10^{-8} mol cm^{-2} s^{-1}. This confirms that with the introduction of the U/P layer, the abundant quaternary ammonium groups in the functional layer generate pronounced electrostatic repulsion. Moreover, the regular pore structure of the MOFs, combined with the anchored amino groups, enables a synergistic sieving mechanism. Li^+, with its lower hydration energy, is facilitated through the pores, whereas Mg^{2+}, with higher hydration energy, is effectively impeded by a combination of steric hindrance and electrostatic repulsion from the amino groups. In other words, UiO-66-NH_2 provides a selective transport pathway for Li^+. Due to their minimal repulsion within the functionalized pores, Li^+ is preferentially conducted, resulting in a significantly enhanced Li^+ flux and a concurrent reduction in Mg^{2+} flux. Increasing the interfacial polymerization reaction time, which directly controls the functional layer thickness, resulted in a marked enhancement of membrane performance. The perm-selectivity increased dramatically from 6.6 to 32.2, accompanied by a significant rise in Li^+ flux from 1.29×10^{-8} mol m^{-2} s^{-1} to 1.59×10^{-8} mol m^{-2} s^{-1}. This phenomenon is attributed to the progressive thickening of the surface PDADMAc layer with extended reaction time, which increasingly impedes the transport of Mg^{2+} ions. Additionally, the MOF channels attached to the membrane surface increase over time, providing more pathways for Li^+ transport. Consequently, the Li^+ flux increases while the Mg^{2+} flux decreases. A comparative study of ion selectivity was conducted between the synthesized membranes and two commercially available references. The results showed that SPES/PEI/U/P-30 exhibited the highest perm-selectivity ($P_{Li^+/Mg^{2+}} = 32.2$), far exceeding that of the commercially available CIMS ($P_{Li^+/Mg^{2+}} = 1.8$) and FUJI CEM ($P_{Li^+/Mg^{2+}} = 1.4$). The aforementioned findings collectively demonstrate the robust performance of the custom-developed ion-exchange membrane under operational conditions of 2.5 mA cm^{-2}.

Regarding the concern that prolonged reaction times may lead to an excessively thick functional layer, the flux and perm-selectivity suggest that any increased transport resistance is more than compensated for by the enhanced ion transport pathways provided by the greater quantity of incorporated MOFs. A closer examination of the flux reveals a nuanced picture: while Li^+ flux rises, the Mg^{2+} flux for SPES/PEI/U/P-5 is actually higher than that of SPES/PEI-2. This suggests a sub-optimal PDADMAc content in the composite membrane, which is insufficient to impart strong electrostatic repulsion. The resulting weak repulsion barrier allows substantial Mg^{2+} permeation. However, this trade-off is offset by a significantly enhanced Li^+ flux, leading to an overall improvement in selectivity.

At higher current densities, the enhanced driving force for ion transport results in a general increase in ion flux. As illustrated in the figure, under the same reaction time, both Li^+ and Mg^{2+} fluxes rise significantly compared to those at lower current densities. Specifically, the Li^+ flux increases to 1.63×10^{-8} mol cm^{-2} s^{-1}, while the Mg^{2+} flux increases to 1.47×10^{-8} mol cm^{-2} s^{-1}. Although the Mg^{2+} flux exhibits a more pronounced upward trend relative to that of Li^+—which may not be considered a favorable outcome—the resulting Mg^{2+}/Li^+ separation perm-selectivity still reaches 13.8 at the higher current density. This indicates that the membrane maintains a discernible separation capability even under intensified operating conditions. It is noteworthy that the significant rise in Mg^{2+} flux may be attributed to the limited positive charge intensity provided by the amino groups in the MOF. Furthermore, consistent with the trade-off effect, this notable increase in Mg^{2+} flux does lead to a considerable decline in selectivity. However, in practical applications, higher current densities are typically employed with larger membrane areas to maintain overall process efficiency. Therefore, despite the observed reduction in perm-selectivity, the membrane still demonstrates excellent perm-selectivity performance under such elevated current density conditions, confirming its practical relevance.

For the long-term stability of this series of membranes, after obtaining the results, we conducted five-cycle long-term stability tests on three types of membranes—SPES-1, SPES/PEI-2, and SPES/PEI/U/P-30—and presented the variations in their selectivity in Fig. 5 and the SI (Fig. S7). After five cycles (each cycle lasting three hours), the obtained data showed that the selectivity of this series of membranes did not exhibit significant fluctuations, indicating that the changes in their performance were not substantial and that they possessed good long-term stability. This also provides a prerequisite for maintaining stable performance during repeated and prolonged testing of these membranes.

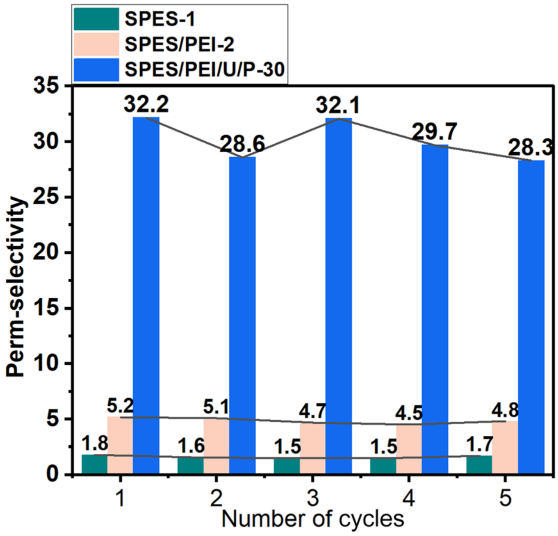

Fig. 5 Selectivity variations of the membrane series after five cycles.

2.5 Evaluation of the perm-selectivity of Na^+ (2.5 mA cm^{-2})

In the sodium–magnesium (Na^+/Mg^{2+}) system, the selectivity trend for the monovalent ion (Na^+) was found to be consistent with that observed in the magnesium–lithium system. The Na^+ perm-selectivity was systematically enhanced with the increased thickness and adhesion degree of the functional layer. The SPES/PEI/U/P-30 membrane achieved the highest perm-selectivity of 26.2, demonstrating that the fabricated functional membrane also possesses excellent monovalent ion selectivity across different ion systems (Fig. 6).

Regarding the ion flux, Na^+ flux increased with the development of the functional layer, whereas Mg^{2+} flux exhibited a concurrent decrease. A maximum Na^+ flux of 1.48×10^{-8} mol cm^{-2} s^{-1} was achieved, which is indicative of the membrane's high permeability in the Na^+/Mg^{2+} system. Similar to Li^+, Na^+ transport is facilitated through the MOF pores. This pathway significantly enhances the migration rate of Na^+, ultimately contributing to the considerable sodium–magnesium perm-selectivity.

Although the monovalent ion selectivity for Na^+ is slightly lower than that for Li^+ (relative to Mg^{2+}), this discrepancy is attributed to competitive hydration effects and differing ion-membrane affinities. The lower charge density and weaker membrane affinity of Na^+ make it more susceptible to competitive displacement and channel blockage by Mg^{2+} ions. Furthermore, the sulfonic acid groups within the membrane exhibit a stronger affinity for Li^+ than for Na^+, facilitating a higher permeation rate of Li^+.[44] Collectively, these factors result in a lower Na^+/Mg^{2+} perm-selectivity compared to the Li^+/Mg^{2+} perm-selectivity.

In assessing the effectiveness of the MOF channels, the flux data offer compelling evidence. The incorporation led to a significant and consistent increase in the fluxes of both Li^+ and Na^+. This observable trend corroborates the successful synthesis of the MOF pores and their varying populations within the membrane matrix.

2.6 Mechanism analysis of monovalent ion perm-selectivity and performance comparison with previous studies

For SPES/PEI/U/P-*n*, we summarize their selective sieving mechanism for monovalent ions as the dual effects of electrostatic repulsion and pore size sieving. Specifically, upon contact with the U/P functional layer of the membrane, Mg^{2+}, bearing a higher charge density, experiences stronger

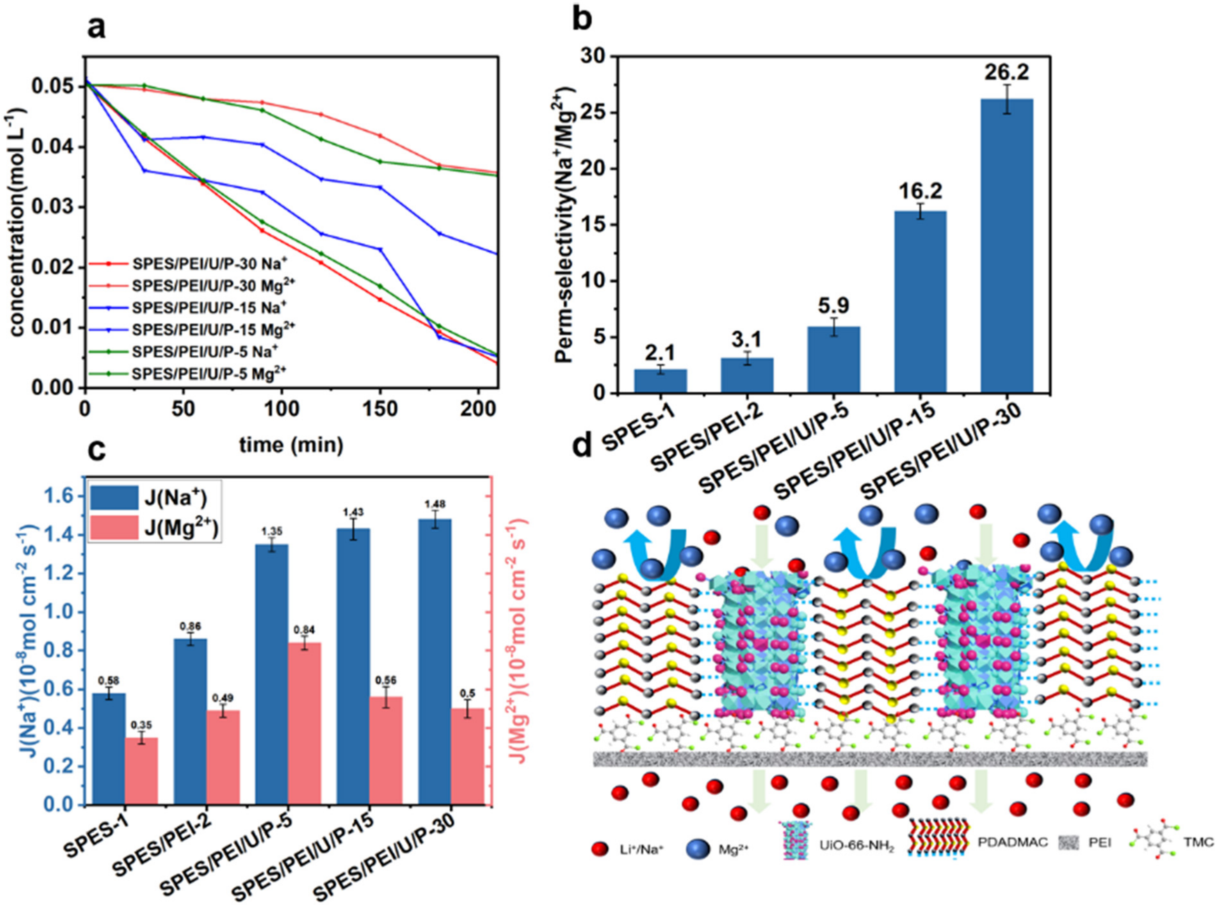

Fig. 6 (a) Concentration evolution of Na^+ and Mg^{2+} ion in DC of EDs fabricated with SPES/PEI/U/P-*n* in different reaction times. (b) Perm-selectivity of different membrane materials in the Na^+/Mg^{2+} system; (c) ion flux of Na^+ and Mg^{2+} in ED; (d) schematic diagram of monovalent ion sieving.

electrostatic repulsion from the PDADMAc layer, which is rich in positively charged quaternary ammonium groups. During transmembrane transport, ions preferentially migrate along pathways of lower electrostatic potential or reduced energy barriers. In this membrane system, the strong electrostatic repulsion generated by the quaternary ammonium groups diverts both ion species toward the MOF channels, where the repulsive force is comparatively weaker. Furthermore, the amino groups and the well-defined pore structures within the UiO-66-NH_2 framework also exert a considerable repulsive force on Mg^{2+} (BET analysis data also exhibit well-defined pore channel data conforming to the separation rule). Consequently, these channels present a significantly lower energy barrier for Li^+ transport relative to Mg^{2+}, enabling selective permeation. Thus, these functionalized pores act as highly selective pathways that preferentially facilitate Li^+ transport, which translates into a significantly higher Li^+ flux compared to that of Mg^{2+}. A similar principle applies to Na^+, which encounters lower transport resistance than Mg^{2+}. However, the transport of Na^+ is less efficient than that of Li^+ due to competitive interference from Mg^{2+} ions.[44] This competition ultimately results in a slightly lower perm-selectivity for the Na^+/Mg^{2+} system relative to the Li^+/Mg^{2+} system. In addition, the PEI interlayer incorporated into the membrane possesses a high density of amino groups, providing substantial electrostatic repulsion. This feature allows it to function as a secondary barrier, effectively intercepting ions that may permeate through the primary U/P functional layer. In general, we attribute the sieving mechanism in this study to the varying magnitudes of electrostatic repulsion experienced by different ions, which drive ions to migrate toward the constructed ion channels with lower resistance. Meanwhile, the functionality of these ion channels can also hinder unwanted ions, thereby achieving selective sieving of monovalent and multivalent ions.

At the molecular scale, simulation analyses of the ion permeation process through UIO-66-NH_2, as reported in the literature, reveal that under an applied electric field, the migration rate of Mg^{2+} exceeds that of Li^+.[45] This phenomenon is likely attributable to the higher positive charge of Mg^{2+}, which results in a stronger electrophoretic driving force. However, despite this higher mobility, Mg^{2+} ions are restricted to the surface region of UIO-66-NH_2 and fail to penetrate into the bulk phase. Consequently, although Li^+ exhibits a lower migration rate and flux, its lower charge

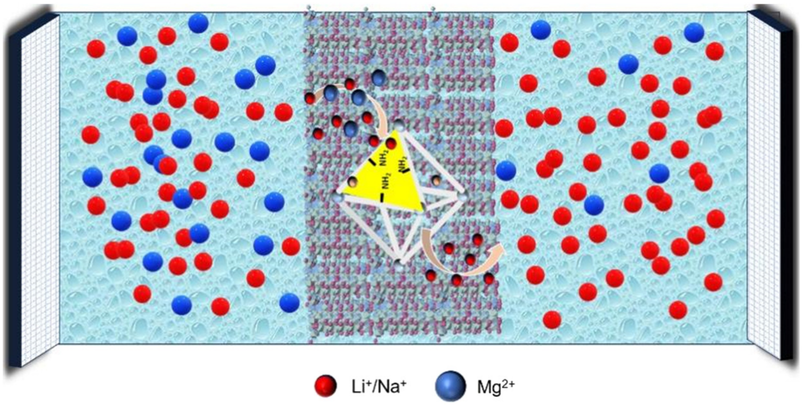

Fig. 7 The transport processes of Li^+/Na^+ and Mg^{2+} in aqueous phase systems.

density subjects it to weaker electrostatic repulsion from the UIO-66-NH_2 framework, thereby facilitating greater passage through the functional layer.[45]

Regarding the transport mechanisms within the UIO-66-NH_2 pores, the brush-like amino groups are proposed to promote all types of ion hopping for Li^+, enhancing its overall transport performance.[46] Furthermore, Li^+ experiences an additional driving force from electrostatic repulsion, accelerating its transit through the nanochannels. In contrast, the binding energy between the amine nitrogen atoms and Mg^{2+} is insufficient to disrupt the tightly bound hydration shell surrounding Mg^{2+} ion clusters. As a result, the amine functional groups present a physical barrier to hydrated Mg^{2+} ions, hindering their transport through the UIO-66-NH_2 framework.[45]

Furthermore, the performance of the membrane developed in this work was benchmarked against other reported membranes in similar studies (Fig. 7). The comparison demonstrates that our membrane exhibits excellent perm-selectivity along with superior Li^+ permeability. This enhanced performance can be attributed to the well-suited pore size of the MOF filler and the strong electrostatic repulsion provided by the polyelectrolyte. As summarized in Table S3, these features collectively contribute to a significant improvement in overall separation performance compared to existing materials.

3 Conclusions

In this study, a UiO-66-NH_2/PDADMAc composite membrane fabricated *via* interfacial polymerization exhibits high Li^+/Mg^{2+} perm-selectivity by synergizing size exclusion and electrostatic repulsion. During ED, the channel diameter of UIO-66-NH_2 better matches Li^+ transport, but blocks Mg^{2+} transport. Its amino groups also provide a certain positive repulsion effect for MOFs, while the PDADMAc polyelectrolyte layer containing quaternary amine groups provides a stronger electrostatic repulsion for Mg^{2+} in the ion exchange process. The hydrogen bonding forces formed by the MOF and the polyelectrolyte bind the two materials tightly together to form a thin, defect-free selective functional layer. As a result, the highest

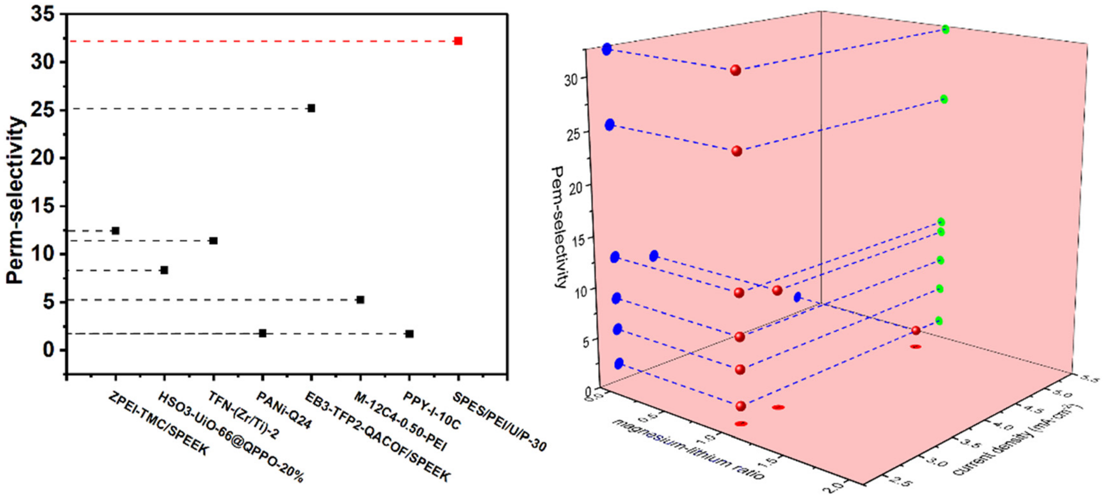

Fig. 8 Comparison of the perm-selectivity of membranes for Mg^{2+}/Li^+ separation *via* ED in different studies.

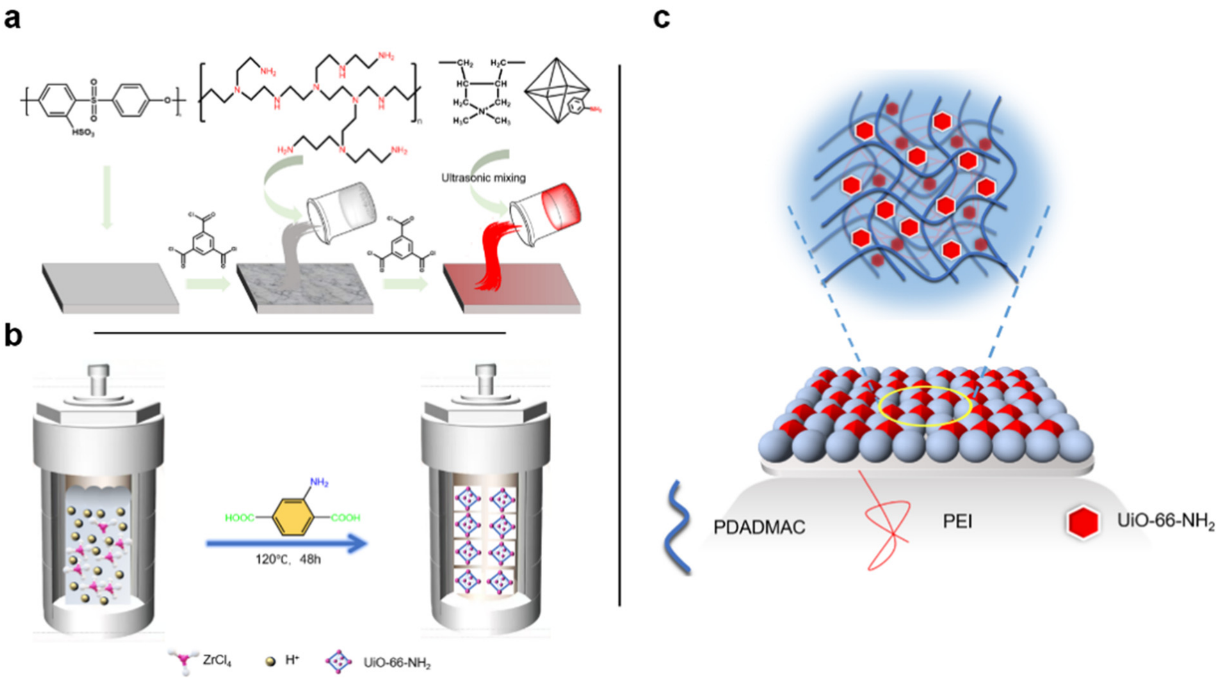

Fig. 9 (a) Route for the preparation of SPES/PEI/U/P-*n* ion exchange membranes; (b) synthesis process of UiO-66-NH_2; (c) schematic diagram of SPES/PEI/U/P-*n* ion exchange membranes.

permeation flux of Li^+ is 1.59×10^{-8} mol cm^{-2} s^{-1}, and the corresponding permeation flux of Mg^{2+} is 0.40×10^{-8} mol cm^{-2} s^{-1} and $P_{Li^+/Mg^{2+}}$ is 32.2 in 210 min. This work demonstrates that MOF–polymer synergistic effects enhance mass transfer resistance, providing a new design strategy for electrodialysis membranes targeting Li^+/Mg^{2+}separation (Fig. 8).

4 Experimental section

4.1 Materials

Polyethyleneimine (PEI) with a molecular weight of 70 000 was from Shanghai Aladdin Reagent Company, polyethersulfone (PES) polymer was from Zhejiang Baichen Low Carbon Technology Co., Ltd., poly(diallyldimethylammonium chloride) (PDADMAc) was from Guangzhou Chemical Reagent Company, 1,3,5-benzenetricarbonyl chloride (TMC) was received from Tianjin C&S Biochemical Technology Co., Ltd., hexane was purchased from Sinopharm Group Chemical Reagent Co., Ltd., *N*,*N*-dimethyl formamide, *N*-methyl pyrrolidone, and *N*,*N*-dimethylacetamide were received from Shanghai Minrel Biochemical Technology Co., Ltd., sulfuric acid (98%) was purchased from Sinopharm Chemical Reagent Co., Ltd, magnesium chloride and lithium chloride were received from Shanghai Titan Technology Co., Ltd., commercial monovalent selective CEM (NEOSEPTA CIMS) and conventional AEM (NEOSEPTA AMX, ASTOM Co., Ltd., Japan) were all purchased from ASTOM Co. General cation exchange membranes were from FUJI Group Japan (Fig. 9).

4.2 Preparation of the SPES base membrane

The sulfonation process of PES is carried out using the following method:[33] 10.0 g of PES polymer was added to 100 mL of DMAc, followed by the addition of approximately 15 mL of concentrated sulfuric acid. The mixture was heated at 70 °C for 10.5 hours, after which the polymer solution was slowly poured into water to be converted into a solid polymer material. The solid polymer material was subsequently dried at 60 °C. Subsequently, 4.0 g of dried SPES polymer was taken and added to 60 mL of NMP. The mixture was heated and stirred to dissolve the polymer. Afterwards, 15 mL of the polymer solution was taken and poured onto a custom-made glass

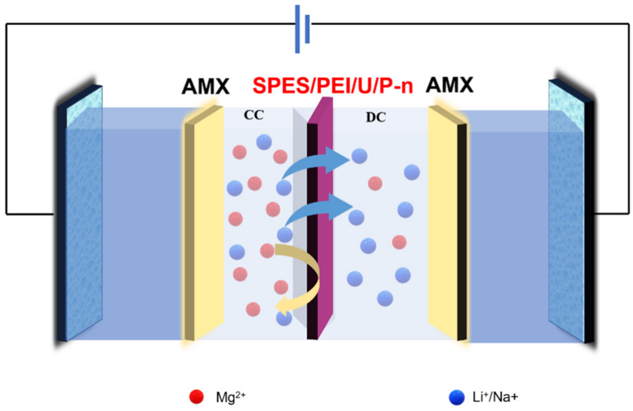

Fig. 10 Membrane configuration of monovalent cation perm-selectivity.

plate, which was then vacuum-dried at 70 °C for 24 hours. The resulting membrane was named SPES-1 (Fig. 10).

4.3 Synthesis of UiO-66-NH$_2$ MOFs

The synthesis of UiO-66-NH$_2$ was carried out by referring to the method in prior work.[36,37] 0.45 g 2-aminoterephthalic acid was taken with 40 mL NMP and 10 mL HCl ultrasound for 30 minutes. 0.58 g ZrCl$_4$ and 50 mL NMP were added into another beaker, and the mixture was added into a high pressure reactor lined with Teflon after being mixed uniformly, sealed and reacted at 120 °C for 48 h. After that, the product was collected by vacuum filtration, washed thoroughly with NMP and water (three times each), and finally dried in a vacuum oven at 60 °C for 24 hours, yielding a dark red powder.

4.4 Preparation of the PEI supporting layer

PEI, which served as a supporting layer for the subsequent attachment of the U/P(UiO-66-NH$_2$/PDADMAc) functional layers, was achieved through the reaction between acyl chloride and amino groups to form amide bonds. 0.66 g TMC was dissolved in 100 mL *n*-hexane solution to form the oil phase and the water phase is the PEI (molecular weight 70 000) solution dissolved in 100 mL of DI water. The prepared SPES-1 membrane was then soaked in the oil phase (TMC/*n*-hexane) and water phase (PEI) in sequence. Generally, the reaction process was carried out thoroughly with a soaking time of 10 minutes; that is, the substrate membrane material was soaked in the oil phase for 10 minutes. It was then taken out and put into the PEI aqueous solution for the same reaction for ten minutes. The reaction of PEI and TMC formed a uniform white PEI functional receiving layer on the membrane surface. The membrane was washed with DI water (deionized water), and air-dried at room temperature until a completely dry surface was achieved. The obtained membrane was named SPES/PEI-2.

4.5 Preparation of SPES/PEI CEMs with UiO-66-NH$_2$/PDADMAc functional

The amine-rich PEI interlayer was cross-linked with the UiO-66-NH$_2$/PDADMAc layer. 250 mg of UiO-66-NH$_2$ powder was ultrasonically dissolved into 100 mL of DI water for 30 min to homogenize. 1.0 g of PDAMDAc was added into the mix, and then mixed, followed by 30 minute ultrasonication to form a uniform, viscous suspension. 0.66 g of TMC was dissolved in 100 mL *n*-hexane. The SPES/PEI-2 membrane was immersed sequentially in two clean glass dishes containing the oil phase (TMC/*n*-hexane) and the UiO-66-NH$_2$/PDADMAc solution. After the reaction, the membrane was retrieved, rinsed with DI water, and air-dried at room temperature. The finally obtained membranes were named SPES/PEI/U/P-5, SPES/PEI/U/P-15 and SPES/PEI/U/P-30 according to the reaction time (U/P-*n*, where *n* represents the reaction time).

4.6 Characterization of materials

The surface morphology of the prepared membrane materials was observed and characterized using a cold-field scanning electron microscope (SEM, Zeiss Gemini 500, Germany). In addition, to enhance the observation of the surface morphologies of the original membrane and modified membranes, the surface morphology of the modified membranes was scanned using a Dimension Icon microscope (Bruker Co.). For the characterization of the chemical structure of the membranes, attenuated total reflection Fourier transform infrared spectroscopy (ATR-FTIR, Nicolet 6700) and X-ray photoelectron spectroscopy (XPS) with a Kratos Axis Ultra DLD spectrometer (Kratos Analytical, Shimadzu, Japan) were employed to analyze the chemical composition of the ion exchange membranes. To characterize the morphology of the synthesized MOF, a cold-field scanning electron microscope (SEM, Zeiss Gemini 500, Germany) was employed to capture detailed images of the individual particles. Additionally, in order to evaluate its crystallinity, X-ray diffraction (XRD) analysis was conducted, Furthermore, to characterize the pore size and dimensional properties of MOFs, a gas adsorption analyzer was employed to obtain the Brunauer–Emmett–Teller (BELSORP MaxII) isotherms and pore size distribution of the MOF materials. The corresponding images are provided in the SI. Furthermore, to characterize the physical properties of the membranes, tests including ion exchange capacity (IEC), water uptake, swelling ratio, electrical resistance, limiting current density and water contact angle were conducted[35] (see SI for detailed procedures).

4.7 Test of monovalent cations perm-selectivity

Perm-selectivity (P), a core indicator for measuring the separation system's ability, is a quantitative description of the difference in migration or distribution behavior between the two ions in the separation system. In this work, we define perm-selectivity as the ratio of the differences in migration amount and migration rate between Li^+ and Mg^{2+} (with Li^+ as the reference relative to Mg^{2+}, and $P_{Na^+/Mg^{2+}}$ is for Na^+ and Mg^{2+}). The test procedure employed a custom-designed device consisting of four compartments, each containing different solutions. The left and right compartments adjacent to the electrodes contained 0.3 M Na_2SO_4 solution (for the Na^+/Mg^{2+} system test, 0.3 M KCl was used) as the circulating electrode solution, while the two middle compartments held the test solutions. To evaluate the selective separation performance of the membrane under relatively high current densities, tests were conducted at two current densities: 2.5 mA cm^{-2} and 5 mA cm^{-2}. At a current density of 2.5 mA cm^{-2}, both the concentrate compartment (CC) and the dilute compartment (DC) contained a 0.05 mol L^{-1} mixed solution of LiCl and $MgCl_2$ (for the Na^+/Mg^{2+} system, the mixed solution was composed of NaCl and $MgCl_2$). At a current density of 5 mA cm^{-2}, the DC contained a 0.05 mol L^{-1} mixed solution of LiCl and $MgCl_2$, and the CC contained a 0.1 mol

L^{-1} KCl solution. During the test, 500 μL samples were collected from the DC solution every 30 minutes over a total duration of 210 minutes. The ion flux and perm-selectivity were calculated in accordance with eqn (1) and (2).[34]

$$J_{\mathrm{i}} = \frac{V}{A_{\mathrm{m}}}\frac{\mathrm{d}C_{\mathrm{i}}}{\mathrm{d}t} \tag{1}$$

$$P = \frac{J^{m+}}{J^{n+}}\frac{C^{m+}}{C^{n+}} \tag{2}$$

where J_{i} represents the mass transfer flux of ions (in mol $\mathrm{cm}^{-2}\ \mathrm{s}^{-1}$), V represents the volume of feed liquid (in cm^3, $V = 80\ \mathrm{cm}^3$), A_{m} represents the effective mass transfer area (in cm^2, $A_{\mathrm{m}} = 19.625\ \mathrm{cm}^2$), and $\mathrm{d}C_{\mathrm{i}}/\mathrm{d}t$ represents the variation trend of ion concentration in DC every 30 minutes.

Author contributions

Tong Mu: conceptualization, data curation, formal analysis, funding acquisition, investigation, methodology, project administration, writing – original draft; Geting Xu: data curation, project administration, software, writing – original draft, writing – review & editing; Zhihang Xia: data curation, project administration; Hao Qian: data curation, formal analysis, methodology; Yangbo Qiu: writing – original draft, writing – review & editing; Wanji Zhou: formal analysis, investigation, methodology; Jiahao Yu: methodology, resources; Yunfang Gao: data curation, software; Junbin Liao: data curation, funding acquisition, investigation; Jiangnan Shen: conceptualization, data curation, formal analysis, writing – original draft.

Conflicts of interest

The authors declare that they have no known competing financial interests or personal relationships that could have appeared to influence the work reported in this paper.

Data availability

The data of this article have been included in this published article and its supplementary information (SI). Further information and data will be made available upon request.

Supplementary information is available. See DOI: https://doi.org/10.1039/d6im00020g.

Acknowledgements

The authors acknowledge the financial support provided by Construction project of National Engineering Research Center for Liquid Separation Membranes (2024ZY01048), the Open Project of Salt Lake Chemical Engineering Research Complex, Qinghai University (2025-DXSSKF-Z02) and the National Natural Science Foundation of China (Grant No. 21878273 and. 22008214). The authors thank Analysis and Testing Center at Zhejiang University of Technology for the assistance in this work.

References

1 M. Zhu, X. Zhao, R. Yan and J. Zhang, Recent research progress of alloy-containing lithium anodes in lithium-metal batteries, *Curr. Opin. Solid State Mater. Sci.*, 2023, **27**, 101079.

2 X. Zhang, S. Huang, M. Xiao, S. J. Wang, Y. Z. Meng and D. M. Han, Designing and constructing stable lithium metal anode by three-dimensional current collector modification with ultralow platinum, *J. Power Sources*, 2025, **631**, 236200.

3 P. Xu, J. Hong, X. M. Qian, Z. W. Xu, H. Xia, X. C. Tao, Z. Z. Xu and Q. Q. Ni, Materials for lithium recovery from salt lake brine, *J. Mater. Sci.*, 2021, **56**(1), 16–63.

4 Y. B. Zheng, Research on Application Fields and Prospect of Lithium, Energy Metal of 21th Century, *Metal World*, 2022(5), 38–45.

5 X. H. Li, Y. H. Mo, W. H. Qing, S. L. Shao, C. Y. Tang and J. X. Li, Membrane-based technologies for lithium recovery from water lithium resources: A review, *J. Membr. Sci.*, 2019, **591**, 117317.

6 S. S. Xu, J. F. Song, Q. Y. Bi, Q. Chen, W.-M. Zhang, Z. X. Qian, L. Zhang, S. A. Xu, N. Tang and T. He, Extraction of lithium from Chinese salt-lake brines by membranes: Design and practice, *J. Membr. Sci.*, 2021, **635**, 119441.

7 C. Grosjean, P. H. Miranda, M. Perrin and P. Poggi, Assessment of world lithium resources and consequences of their geographic distribution on the expected development of the electric vehicle industry, *Renewable Sustainable Energy Rev.*, 2012, **16**(3), 1735–1744.

8 X. C. Yin, P. Xu and H. Y. Wang, Modification of cation exchange membranes for enhanced extraction of lithium from magnesium and sodium brine solutions via selective electrodialysis, *J. Membr. Sci.*, 2024, **701**, 122705.

9 X. Li, Y. Mo, W. Qing, S. Shao, C. Y. Tang and J. Li, Membrane-based technologies for lithium recovery from water lithium resources: A review, *J. Membr. Sci.*, 2019, **591**, 117317.

10 Y. Sun, Q. Wang, Y. H. Wang, R. P. Yun and X. Xiang, Recent advances in magnesium/lithium separation and lithium extraction technologies from salt lake brine, *Sep. Purif. Technol.*, 2021, **256**, 117807.

11 N. Linneen, R. Bhave and D. Woerner, Purification of industrial grade lithium chloride for the recovery of high purity battery grade lithium carbonate, *Sep. Purif. Technol.*, 2019, **214**, 168–173.

12 G. Liu, Z. W. Zhao and L. H. He, Highly selective lithium recovery from high Mg/Li ratio brines, *Desalination*, 2020, **474**, 114185.

13 Y. J. Zhao, H. Y. Wang, Y. Li, M. Wang and X. Xiang, An integrated membrane process for preparation of lithium hydroxide from high Mg/Li ratio salt lake brine, *Desalination*, 2020, **493**, 114620.

14 C. Grosjean, P. H. Miranda, M. Perrin and P. Poggi, Assessment of world lithium resources and consequences of their geographic distribution on the expected development of the electric vehicle industry, *Renewable Sustainable Energy Rev.*, 2012, **16**(3), 1735–1744.

15 Y. Zhang, Y. H. Hu, L. Wang and W. Sun, Systematic review of lithium extraction from salt-lake brines via precipitation approaches, *Miner. Eng.*, 2019, **139**, 105868.

16 X. H. Liu, M. L. Zhong, X. Y. Chen and Z. W. Zhao, Separating lithium and magnesium in brine by aluminum-based materials, *Hydrometallurgy*, 2018, **176**, 73–77.

17 Z. H. Xu, H. J. Zhang, R. Y. Wang, W. J. Gui, G. F. Liu and Y. Yang, Systemic and Direct Production of Battery-Grade Lithium Carbonate from a Saline Lake, *Ind. Eng. Chem. Res.*, 2014, **53**(42), 16502–16507.

18 P. Meshram, B. D. Pandey and T. R. Mankhand, Extraction of lithium from primary and secondary sources by pre-treatment, leaching and separation: A comprehensive review, *Hydrometallurgy*, 2014, **150**, 192–208.

19 J. W. An, D. J. Kang, K. T. Tran, M. J. Kim, T. Lim and T. Tran, Recovery of lithium from Uyuni salar brine, *Hydrometallurgy*, 2012, **117–118**, 64–70.

20 X.-Y. Nie, S.-Y. Sun, Z. Sun, X. F. Song and J.-G. Yu, Ion-fractionation of lithium ions from magnesium ions by electrodialysis using monovalent selective ion-exchange membranes, *Desalination*, 2017, **403**, 128–135.

21 L. J. Banasiak, T. W. Kruttschnitt and A. I. Schäfer, Desalination using electrodialysis as a function of voltage and salt concentration, *Desalination*, 2007, **205**(1), 38–46.

22 B. Y. Wang, R. R. Li, Z. Z. Cui, Z. H. Wang, W. C. Fu, J. Y. Yan, C. X. Jiang, L. Wu, T. W. Xu and Y. M. Wang, Facile design of a crown ether-functionalized polymeric membrane for highly efficient lithium and magnesium separation during electrodialysis, *Chem. Eng. Sci.*, 2025, **302**, 120865.

23 Y. Y. Liu, R. Zhu, C. Srinivasakannan, T. T. Li, S. W. Li, S. H. Yin and L. B. Zhang, Application of Nanofiltration Membrane Based on Metal-Organic Frameworks (MOFs) in the Separation of Magnesium and Lithium from Salt Lakes, *Separations*, 2022, **9**(11), 344.

24 P. Hu, B. B. Yuan, Q. J. Niu, N. Wang, S. H. Zhao, J. B. Cui and J. H. Jiang, In situ assembled zeolite imidazolate framework nanocrystals hybrid thin film nanocomposite membranes for brackish water desalination, *Sep. Purif. Technol.*, 2022, **293**, 121134.

25 L. M. Robeson, Q. Liu, B. D. Freeman and D. R. Paul, Comparison of transport properties of rubbery and glassy polymers and the relevance to the upper bound relationship, *J. Membr. Sci.*, 2015, **476**, 421–431.

26 Z. G. Hu, Y. H. Peng, Y. J. Gao, Y. H. Qian, S. M. Ying, D. Q. Yuan, S. Horike, N. Ogiwara, R. Babarao, Y. X. Wang, N. Yan and D. Zhao, Direct Synthesis of Hierarchically Porous Metal–Organic Frameworks with High Stability and Strong Brønsted Acidity: The Decisive Role of Hafnium in Efficient and Selective Fructose Dehydration, *Chem. Mater.*, 2016, **28**(8), 2659–2667.

27 X. J. Zeng, L. Xu, T. Deng, Y. X. Wang, W. Xu and W. Zhang, Anionic MOFs Embedded in Anion-Exchange Membranes for the Separation of Lithium/Magnesium Cations, *ACS Sustainable Chem. Eng.*, 2023, **11**(35), 12877–12887.

28 T. T. Xu, F. M. Sheng, B. Wu, M. A. Shehzad, A. Yasmin, X. X. Wang, Y. B. He, L. Ge, X. S. Zheng and T. W. Xu, Ti-exchanged UiO-66-NH_2–containing polyamide membranes with remarkable cation permselectivity, *J. Membr. Sci.*, 2020, **615**, 118608.

29 M. Kalaj, K. C. Bentz, S. Ayala, J. M. Palomba, K. S. Barcus, Y. Katayama and S. M. Cohen, MOF-Polymer Hybrid Materials: From Simple Composites to Tailored Architectures, *Chem. Rev.*, 2020, **120**(16), 8267–8302.

30 M. S. Denny Jr and S. M. Cohen, In Situ Modification of Metal–Organic Frameworks in Mixed-Matrix Membranes, *Angew. Chem., Int. Ed.*, 2015, **54**(31), 9029–9032.

31 J. J. Wang, H. Zhang, R. K. Tian, H. Y. Shen, W.-H. Li and Y. K. Wang, Enhancing Mg^{2+}/Li^{+} separation performance of nanofiltration membranes through polyelectrolyte modulation and surface modification, *J. Membr. Sci.*, 2024, **701**, 122725.

32 A. K. Thakur, M. Manohar and V. K. Shahi, Controlled metal loading on poly(2-acrylamido-2-methyl-propane-sulfonic acid) membranes by an ion-exchange process to improve electrodialytic separation performance for mono−/bi-valent ions, *J. Mater. Chem. A*, 2015, **3**(35), 18279–18288.

33 J. L. Zhao, L. Guo and J. Y. Wang, Synthesis of cation exchange membranes based on sulfonated polyether sulfone with different sulfonation degrees, *J. Membr. Sci.*, 2018, **563**, 957–968.

34 Q. Chen, Y. Y. Yao, J. B. Liao, J. H. Li, J. W. Xu, T. T. Wang, Y. Y. Tang, Y. Q. Xu, H. M. Ruan and J. N. Shen, Subnanometer Ion Channel Anion Exchange Membranes Having a Rigid Benzimidazole Structure for Selective Anion Separation, *ACS Nano*, 2022, **16**(3), 4629–4641.

35 M. Fujimura, T. Hashimoto and H. Kawai, Small-angle x-ray scattering study of perfluorinated ionomer membranes. 1. Origin of two scattering maxima, *Macromolecules*, 1981, **14**(5), 1309–1315.

36 M. Kandiah, M. H. Nilsen, S. Usseglio, S. Jakobsen, U. Olsbye, M. Tilset, C. Larabi, E. A. Quadrelli, F. Bonino and K. P. Lillerud, Synthesis and Stability of Tagged UiO-66 Zr-MOFs, *Chem. Mater.*, 2010, **22**(24), 6632–6640.

37 K. Mirzaei, E. Jafarpour, A. Shojaei, S. S. Khasraghi and P. Jafarpour, An investigation on the influence of highly acidic media on the microstructural stability and dye adsorption performance of UiO-66, *Appl. Surf. Sci.*, 2023, **618**, 156531.

38 S. J. Xu, F. Li, B. W. Su, M. Z. Hu, X. L. Gao and C. J. Gao, Novel graphene quantum dots (GQDs)-incorporated thin film composite (TFC) membranes for forward osmosis (FO) desalination, *Desalination*, 2019, **451**, 219–230.

39 K. Chen, S. C. Zhao, H. L. Lan, T. T. Xie, H. Wang, Y. H. Chen, P. Li, H. X. Sun, Q. Jason Niu and C. H. Yang, Dual-electric layer nanofiltration membranes based on polyphenol/PEI interlayer for highly efficient Mg^{2+}/Li^{+}separation, *J. Membr. Sci.*, 2022, **660**, 120860.

40 A. K. Thakur, M. Manohar and V. K. Shahi, Controlled metal loading on poly(2-acrylamido-2-methyl-propane-sulfonic acid) membranes by an ion-exchange process to improve electrodialytic separation performance for mono−/bi-valent ions, *J. Mater. Chem. A*, 2015, **3**(35), 18279–18288.

41 T. Kim, Y. Kwon, J. Lee, D. Lee, H. S. Shin, M. Cho and S. Kwon, Development of hydrophilicity on the proton

exchange using sulfonic acid on PEEK in the presence of water: a density functional theory study, *Theor. Chem. Acc.*, 2017, **136**(11), 130.

42 J. F. Bai, R. Ding, Y. Y. Wang, T. J. Chen, Q. Z. Xu, B. Feng, K. Duan, W. Zhi, J. Weng and J. X. Wang, Surface modification of polyetheretherketone by grafting amino groups to improve its hydrophilicity and cytocompatibility, *Mater. Res. Express*, 2019, **6**(11), 115413.

43 Z. Z. Xu, J. Y. Liao, H. Tang, J. E. Efome and N. W. Li, Preparation and antifouling property improvement of Tröger's base polymer ultrafiltration membrane, *J. Membr. Sci.*, 2018, **561**, 59–68.

44 G. M. Geise, D. R. Paul and B. D. Freeman, Fundamental water and salt transport properties of polymeric materials, *Prog. Polym. Sci.*, 2014, **39**, 1–42.

45 Y. Lim, Y. Kim and J. Choi, Electro-mechanical factor affecting the Li^+/Mg^{2+} selectivity performance of ion separation metal–organic frameworks, *J. Mater. Chem. A*, 2024, **12**, 16657–16666.

46 H. Xiao, M. Chai, M. Abdollahzadeh, H. Ahmadi, V. Chen, D. B. Gore, M. Asadnia and A. Razmjou, A lithium ion selective membrane synthesized from a double layered Zrbased metalorganic framework (MOF-on-MOF) thin film, *Desalination*, 2022, **532**, 115733.